PNAS RESEARCH ARTICLE | PHYSIOLOGY

KCNH2 encodes a nuclear-targeted polypeptide that mediates hERG1 channel gating and expression

Abhilasha Jain[a], Olivia Stack[a], Saba Ghodrati[b], Francisco G. Sanchez-Conde[a], Chiamaka U. Ukachukwu[a], Shreya Salwi[a], Eric N. Jimenez-Vazquez[a], and David K. Jones[a,c,1]

Edited by Jonathan H. Jaggar, University of Tennessee Health Science Center, Memphis, TN; received August 26, 2022; accepted November 17, 2022 by Editorial Board Member Mark T. Nelson

KCNH2 encodes hERG1, the voltage-gated potassium channel that conducts the rapid delayed rectifier potassium current (I_{Kr}) in human cardiac tissue. hERG1 is one of the first channels expressed during early cardiac development, and its dysfunction is associated with intrauterine fetal death, sudden infant death syndrome, cardiac arrhythmia, and sudden cardiac death. Here, we identified a hERG1 polypeptide ($hERG1_{NP}$) that is targeted to the nuclei of immature cardiac cells, including human stem cell-derived cardiomyocytes (hiPSC-CMs) and neonatal rat cardiomyocytes. The nuclear $hERG1_{NP}$ immunofluorescent signal is diminished in matured hiPSC-CMs and absent from adult rat cardiomyocytes. Antibodies targeting distinct hERG1 channel epitopes demonstrated that the $hERG1_{NP}$ signal maps to the hERG1 distal C-terminal domain. _KCNH2_ deletion using CRISPR simultaneously abolished I_{Kr} and the $hERG1_{NP}$ signal in hiPSC-CMs. We then identified a putative nuclear localization sequence (NLS) within the distal hERG1 C-terminus, 883-RQRKRKLSFR-892. Interestingly, the distal C-terminal domain was targeted almost exclusively to the nuclei when overexpressed HEK293 cells. Conversely, deleting the NLS from the distal peptide abolished nuclear targeting. Similarly, blocking α or β1 karyopherin activity diminished nuclear targeting. Finally, overexpressing the putative $hERG1_{NP}$ peptide in the nuclei of HEK cells significantly reduced hERG1a current density, compared to cells expressing the NLS-deficient $hERG1_{NP}$ or GFP. These data identify a developmentally regulated polypeptide encoded by _KCNH2_, $hERG1_{NP}$, whose presence in the nucleus indirectly modulates hERG1 current magnitude and kinetics.

hERG1 | cardiac physiology | cell biology | KCNH2 | electrophysiology

Significance

KCNH2 encodes the voltage-gated potassium channel, hERG1. hERG1 variants are associated with sudden death in the young, including intrauterine fetal death, sudden infant death syndrome (SIDS), and sudden unexplained death in epilepsy (SUDEP). Here we identify a non-conducting *KCNH2*-encoded polypeptide, $hERG1_{NP}$, that is upregulated in immature cardiomyocytes, and its targeting to the nucleus indirectly modulates hERG1 gating. These data identify a regulatory mechanism for hERG1 channels and could represent a therapeutic target for diseases related to hERG1 dysfunction.

The *KCNH2* gene encodes hERG1, the voltage-gated potassium channel that conducts the critical cardiac repolarizing current, I_{Kr} (1, 2). *KCNH2* variants that reduce $I_{Kr,}$ or off-target hERG1 channel block cause the cardiac disorder long QT syndrome and increase the likelihood for cardiac arrhythmia and sudden cardiac death (2, 3). *KCNH2* variants have also been linked with a number of causes of death in the young that may or may not be directly linked to cardiac dysfunction, including intrauterine fetal death (4), sudden infant death syndrome (SIDS) (5, 6), and sudden unexplained death in epilepsy (7–9).

The *KCNH2* gene encodes multiple hERG1 splice variants in cardiac tissue (10–12). Conducting hERG1 channels comprise at least two subunits encoded by alternate *KCNH2* transcripts, hERG1a and hERG1b, that are identical apart from their N-terminal domains (10, 11). hERG1a contains an N-terminal Per-Arnt-Sim (PAS) domain that regulates gating through dynamic interactions with the S4-S5 linker and the cyclic nucleotide-binding homology domain (CNBHD) of the proximal C-terminus (13–17). hERG1b has a much shorter and unique N-terminus that lacks a functional PAS domain (10, 11). When expressed in HEK293 cells, the absence of a PAS domain in hERG1b accelerates the time course of activation, deactivation, and inactivation recovery of heteromeric hERG 1a/1b channels by twofold, compared to homomeric hERG1a channels (18). In human cardiomyocytes, silencing hERG1b by overexpressing a polypeptide that mimics the hERG1a PAS domain slows native I_{Kr} gating kinetics and reduces I_{Kr} magnitude, prolonging the action potential duration (19). Conversely, disabling the hERG1a PAS domain using PAS-targeting antibodies accelerates I_{Kr} gating, increases I_{Kr} magnitude, and hastens cardiac repolarization (20). *KCNH2* also encodes a non-conducting C-terminal splice variant that reduces total hERG1 current density, $hERG1_{USO}$ (12, 21, 22). $hERG1_{USO}$ can combine with either N-terminal variant (hERG1a vs $hERG1a_{USO}$, & hERG1b vs $hERG1b_{USO}$) (12, 21, 22). The relative abundance of hERG1 subunits shifts during fetal development (4) and heart failure (23), suggesting that hERG1 subunit abundance is dynamic.

Author affiliations: [a]Department of Pharmacology, University of Michigan Medical School, Ann Arbor, MI 48109; [b]University of Texas at San Antonio, San Antonio, TX 78249; and [c]Department of Internal Medicine, University of Michigan Medical School, Ann Arbor, MI 48109

Author contributions: A.J., O.S., S.G., E.N.J.-V., and D.K.J. designed research; A.J., O.S., S.G., F.G.S.-C., C.U.U., S.S., E.N.J.-V., and D.K.J. performed research; C.U.U. and D.K.J. contributed new reagents/analytic tools; A.J., O.S., S.G., F.G.S.-C., S.S., E.N.J.-V., and D.K.J. analyzed data; and E.N.J.-V. and D.K.J. wrote the paper.

The authors declare no competing interest.

This article is a PNAS Direct Submission. J.H.J. is a guest editor invited by the Editorial Board.

[1]To whom correspondence may be addressed. Email: davekj@umich.edu.

This article contains supporting information online at https://www.pnas.org/lookup/suppl/doi:10.1073/pnas.2114700120/-/DCSupplemental.

Published January 10, 2023.

The hERG1 C-terminus is a critical component of hERG1 channel function. The proximal C-terminus (670-872, hERG1a numbering) is highly structured and contains a C-linker and a CNBHD that play integral roles in channel gating (13, 15, 17, 24–29). Mutations throughout the C-linker and CNBHD trigger dramatic changes in hERG1 gating and surface expression (24, 30). In contrast, the distal C-terminal domain (863-1159, hERG1a numbering) is disordered (31, 32) and its contribution to hERG1 function is less clear. In fact, several SIDS-associated hERG1 variants in the distal C-terminus have a limited impact on hERG1 gating or expression (33). Thus, the causal link between many *KCNH2* variants and sudden death in the young remains unclear, and the regulatory mechanisms of hERG1 in immature cardiomyocytes are underexplored.

To identify regulators of hERG1 expression in developing cardiomyocytes, we leveraged the immature nature of human stem cell-derived cardiomyocytes (hiPSC-CMs). hiPSC-CMs display maturation comparable to cardiomyocytes isolated from human embryonic and/or fetal cardiac tissue (34). And with the increasing accessibility of CRISPR technology, hiPSC-CMs are a uniquely powerful tool to explore regulatory mechanisms in immature human cardiomyocytes. Here we identify a non-conducting KCNH2-encoded polypeptide, $hERG1_{NP}$, that is targeted to the nuclei of immature cardiac cells, including hiPSC-CMS and neonatal rat cardiomyocytes, but not adult rat cardiomyocytes. $hERG1_{NP}$ expression within the nucleus reduced hERG1 current density by depolarizing the voltage dependence of activation and stabilizing inactivation. These data identify $hERG1_{NP}$ as a developmentally regulated, *KCNH2*-encoded polypeptide that regulates hERG1 function via the cell's nucleus.

Results

A hERG1 Immunofluorescence Signal in Cardiac Nuclei. To identify regulatory mechanisms of hERG1 function, we cultured human pluripotent stem cell-derived cardiomyocytes (hiPSC-CMs) on Matrigel-coated glass coverslips. We used phalloidin labeling actin to identify cardiomyocytes from other cell types, as previously described (19, 35). We immunolabeled for hERG1 using antibodies targeting two distinct epitopes: 1) the extracellular p-loop and 2) the distal C-terminal domain (Fig. 1*A*). We then measured immunofluorescence using confocal microscopy to track the distribution of the two antibodies, using a DAPI stain to delineate the nuclei. Surprisingly, the immunolabeling pattern of the two antibodies did not overlap. The distribution of the p-loop-targeting antibody was enriched in the cardiac ER, cytoplasmic space, and surface membrane, consistent with previous reports of hERG1 distribution in cardiac cells (36–39). In contrast, the antibody targeting the hERG C-terminal domain was enriched within the nuclei (Fig. 1*B*). To quantify the relative distribution of nuclear vs non-nuclear hERG1 fluorescence, we divided the mean hERG1 fluorescence intensity within the nucleus by the mean fluorescence intensity within the cytoplasm from each cell. The ratio of nuclear to cytoplasmic fluorescence was significantly higher for the C-terminal antibody compared to the p-loop antibody ($P < 0.0001$) (Fig. 1*C*). These data suggest that hiPSC-CMs target a portion of the hERG1 protein to their nuclei.

Nuclear hERG1 Distribution Corresponds With Cardiac Maturation. To determine if these results were an artifact of the in vitro differentiation process, we repeated these experiments in freshly isolated neonatal and adult rat cardiomyocytes (Fig. 1*B*). Antibodies targeting the rERG1 p-loop and C-terminal domain in neonatal rat cardiomyocytes displayed a similar distribution as hERG1 in hiPSC-CMs, where the C-terminal antibody displayed greater nuclear enrichment compared to the p-loop antibody. Interestingly, adult rat myocytes did not display distinct distribution of the p-loop and C-terminal rERG1 antibodies (Fig. 1*C*), and nuclear rERG1 staining was significantly lower in adult rat compared to neonatal rat cardiomyocytes (Fig. 1*D*). Importantly, the distribution of the p-loop antibody was unchanged between neonatal and adult rat cardiomyocytes (Fig. 1*E*). These data suggest that the abundance of nuclear ERG1 is dependent upon the maturation state to the cardiomyocyte.

Cardiomyocytes differentiated from human stem cells and cultured on Matrigel-coated coverslips display characteristics consistent with those observed in human embryonic/fetal cardiomyocytes, including poor sarcomere organization, low cTnI expression, and depolarized resting membrane potentials (19, 34, 40, 41). We evaluated if in vitro hiPSC-CM maturation could reduce the nuclear distribution of the C-terminal hERG1 signal, similarly to that observed between neonatal and adult rat cardiomyocytes. To induce hiPSC-CM maturation, we cultured hiPSC-CMs on a commercial cardiac maturation matrix, MatrixPlus (42). hiPSC-CMs cultured on MatrixPlus display rod-shaped morphology, highly organized sarcomeres, elevated cTnI expression, and resting membrane potentials at or near −80 mV (42). In MatrixPlus-cultured hiPSC-CMs, the C-terminal antibody displayed greater nuclear enrichment compared to the p-loop antibody (Fig. 1 *C* and *D*). However, nuclear hERG1 enrichment was significantly reduced in MatrixPlus-cultured hiPSC-CMs compared to hiPSC-CMs cultured on glass, and more closely resembled rERG1 levels measured from rat neonatal cardiomyocytes (Fig. 1*D*). The distribution of the p-loop antibody was unchanged between glass-cultured and MatrixPlus-cultured hiPSC-CMs (Fig. 1*E*). These data demonstrate that the abundance of the nuclear ERG1 immunofluorescent signal associated with the ERG1 C-terminus is dependent upon the maturation state of the cardiomyocyte.

***KCNH2* Deletion Abolishes the Nuclear hERG1 Immunosignal.** To validate the accuracy of the hERG1 nuclear immunofluorescent signal, we immunolabeled for hERG1 in a line of stem cell-derived cardiomyocytes where *KCNH2* expression was abolished by CRISPR (Fig. 2). Isogenic control and KCNH2-null stem cells displayed markers of pluripotency (Fig. 2*A*) and successfully differentiated into contracting cardiomyocytes displaying the reticulated actin staining corresponding with alignment of the cardiac sarcomeres (Fig. 2*B*). Isogenic control cardiomyocytes conducted I_{Kr} and displayed both cytoplasmic and nuclear hERG1 immunosignals using the C-terminal-targeting antibody. In contrast, *KCNH2* double-null cardiomyocytes cultured on Matrigel-coated glass lacked I_{Kr} and did not display a discernable hERG1 immunosignal in the cytoplasm or nucleus (Fig. 2 *B*–*E*). These data unequivocally validate the specificity of hERG1 immunofluorescent signal in the cardiac nucleus and identify a KCNH2-encoded polypeptide that we termed: $hERG1_{NP}$.

The α/β_1 Karyopherin Complex Regulates $hERG1_{NP}$ Nuclear Transport. The complex between the α and β1 karyopherins mediates the classical nuclear transport pathway (43). To assess if $hERG1_{NP}$ trafficking is dependent upon this pathway, we inhibited α and β1 karyopherin activity using ivermectin and importazole, respectively (44, 45). We incubated hiPSC-CMs in 40 μM importazole for 8 h and then measured the relative nuclear and cytoplasmic distribution of hERG1 using the C-terminal antibody as described above (Fig. 2). 40 μM importazole significantly reduced the relative intensity of the nuclear hERG1

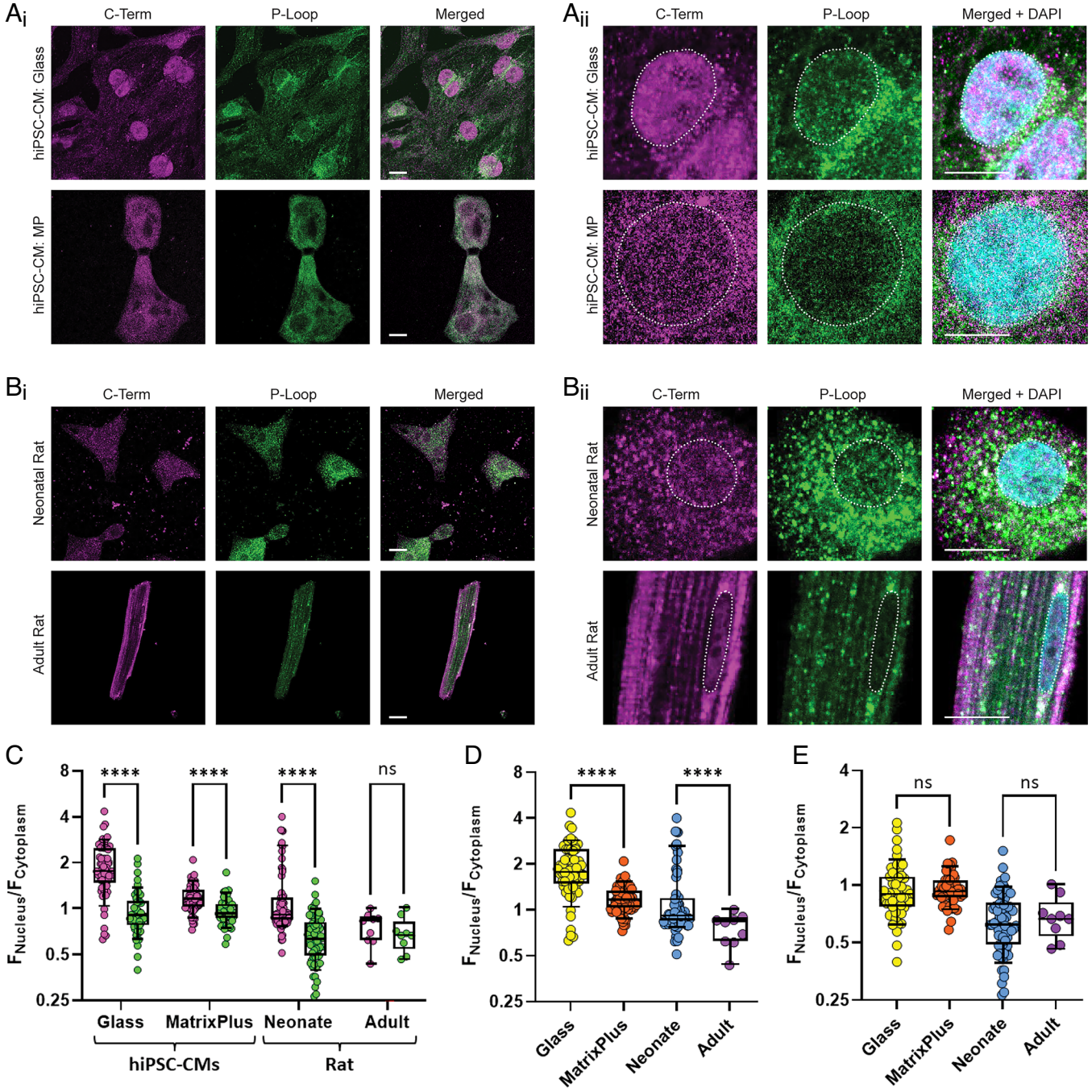

Fig. 1. ERG1 immunofluorescence signal in cardiac nuclei. (A_i and A_{ii}) hiPSC-CMs cultured on glass (*Top*) or Matrixplus (*Bottom*). Cells are dual labeled for hERG1 with antibodies targeting the carboxy terminus (*C-Term*) and the extracellular pore (*P-Loop*). (A_{ii}) Expanded view of select nuclei from images in "A_i." The DAPI stain (*cyan*) is included to mark the nucleus in the merged images. The white dotted line depicts the nuclear boundary in the C-Term and P-Loop images. (B_i and B_{ii}) Cardiomyocytes of neonatal rat (*Top*) or adult rat (*Bottom*) labeled for rERG1 with antibodies as in "*A*." (B_{ii}) Expanded view of select nuclei from images in "B_i." The DAPI stain (*cyan*) is included to mark the nucleus in the merged images. The white dotted line depicts the nuclear boundary in the C-Term and P-Loop images. Scale bars indicate 10 μM. (*C*) Box and whisker plots depicting nuclear fluorescence intensity relative to cytoplasmic fluorescence intensity ($F_{Nucleus}/F_{Cytoplasm}$) for the C-Term and P-loop antibodies. The C-Term antibody was enriched in the nucleus compared to the P-Loop antibody in immature cardiomyocytes, but not adult cardiomyocytes. (*D*) Box and whisker plots demonstrating that the relative abundance of nuclear ERG1 fluorescence of the C-Term antibody ($F_{Nucleus}/F_{Cytoplasm}$) decreased with increased cardiac maturation. (*E*) The intracellular distribution of the P-Loop antibody was unaffected by cardiomyocyte maturation. Paired groups in "*C*" were compared using a Wilcoxon matched-pairs test. Means in "*D*" and "*E*" were compared using a Mann–Whitney test. **** indicates $P < 0.0001$.

signal compared to vehicle controls (Fig. 3), indicating that nuclear transport of the $hERG1_{NP}$ is karyopherin-β1 dependent. To test if $hERG1_{NP}$ trafficking is also dependent upon the α karyopherin, we blocked incubated cells with 2.5 μM ivermectin for 8 h. Like importazole, ivermectin significantly reduced the relative intensity of the nuclear hERG1 signal, compared to vehicle controls (Fig. 3). These data indicate that the classical nuclear transport pathway mediates $hERG1_{NP}$ localization in the nucleus.

A Nuclear Localization Sequence in the Distal C-Terminal Domain of hERG1. Karyopherins recognize and bind to their cargo through monopartite or bipartite nuclear localization sequences (NLS) (46). To determine if hERG1 contains an NLS that may mediate nuclear targeting, we screened the hERG1 amino acid sequence using the open-source software *cNLS Mapper*. *cNLS Mapper* identified a single putative monopartite NLS in the distal hERG1 C-terminal domain (883RQRKRKLSFR892, Fig. 4*A*). This NLS

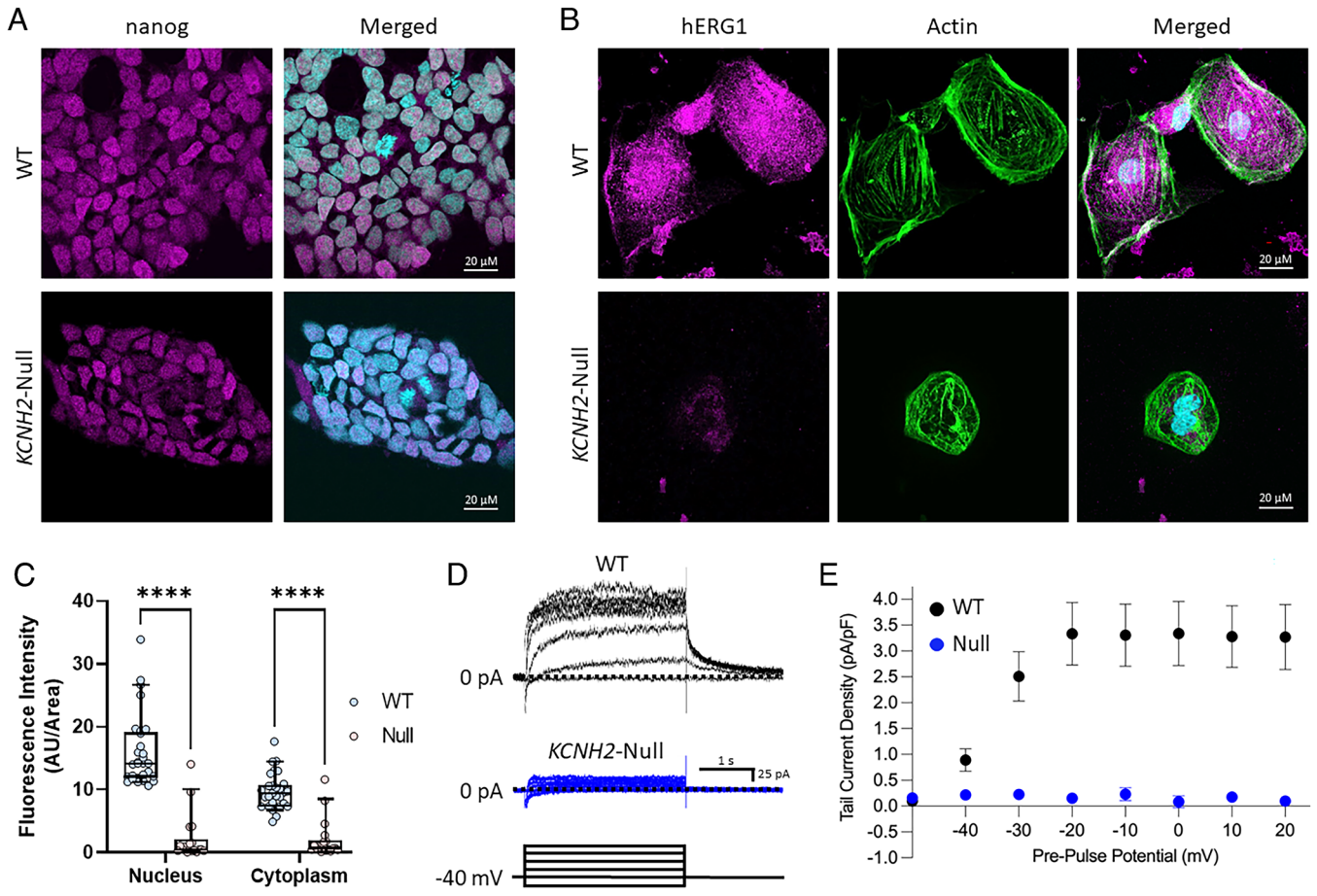

Fig. 2. *KCNH2* deletion abolishes the nuclear hERG1 signal. (*A*) Wildtype isogenic control (WT) and *KCNH2*-null hESCs stained for the pluripotency marker nanog (*magenta*) and DAPI (*cyan*). (*B*) Wildtype isogenic control (WT) and *KCNH2*-null hESC-CMs stained for hERG1 with the C-Term antibody (*magenta*), along with phalloidin (*green*) and DAPI (*cyan*) to mark actin and nuclei, respectively. (*C*) Mean nuclear and cytoplasmic fluorescence recorded from wildtype (WT, *blue*) or *KCNH2*-null (Null, *red*) hESC-CMs. *KCNH2*-null hESC-CMs do not display a nuclear or cytoplasmic hERG1 signal. (*D*) Sample E-4031-sensitve currents, indicative of I_{Kr}, recorded from wildtype isogenic control hES-CMS (*Top, black*) and *KCNH2*-null hESC-CMs (*Bottom, blue*). A schematic depicting the pulse protocol used is depicted at bottom. (*E*) Peak tail I_{kr} density plotted as a function of pre-pulse potential for wildtype isogenic control (*black*) and *KCNH2*-null (*blue*) cardiomyocytes. *KCNH2*-null hES-CMs did not conduct a discernable I_{Kr}. n = 9 and 6 for wildtype and *KCNH2*-null I_{Kr} recordings, respectively. Data are represented as mean ± standard error. Means in "*C*" were compared using a Mann–Whitney test. **** indicates $P < 0.0001$.

is completely absent from the hERG orthologue, hERG2. The sequence is partially conserved in the hERG orthologue hERG3; however, *cNLS Mapper* did not identify the hERG3 sequence as a potential NLS (Fig. 4*B*).

We then used three citrine-fused polypeptides to assess the functionality of the putative hERG1 NLS: 666-1,159, 666-872, and 873-1,159 (Fig. 4*C*). The 666-1,159 construct (full-length-CT) represents the entire hERG1 C-terminal cytoplasmic domain. The 666-872 construct (proximal-CT) forms the hERG1 C-linker and CNBH domains. The 873-1,159 construct (distal-CT) forms the disordered distal C-terminal domain of hERG1. We expressed each fusion peptide individually in HEK293 cells and tracked the distribution of the peptides using confocal microscopy. Cells transfected with the full-length-CT (666-1,159) displayed a bimodal distribution. 81% of cells displayed cytoplasmic enrichment; however, a subset of cells (19%) displayed a strong nuclear enrichment (Fig. 4 *D*, *Top Left*). The proximal-CT (666-872) lacks the NLS sequence and displayed equivalent fluorescence between the cytoplasm and nuclei (Fig. 4 *D*, *Top Right*). In contrast, the distal-CT (873-1,159), which contains the putative NLS, was limited almost exclusively to the cells' nuclei (Fig. 4 *D*, *Bottom Left*). Additionally, deleting the NLS coding region from the distal-CT construct abolished nuclear targeting (ΔNLS, Fig. 4 *C* and *D*, *Bottom Right*), demonstrating that the 883RQRKRKLSFR892 sequence drives nuclear transport of the distal peptide. These results show that the hERG1 sequence 883RQRKRKLSFR892 is a functional NLS.

Finally, to determine if the nuclear targeting of the distal-CT and full-length-CT in HEK293 cells followed the same mechanism as that observed in the hiPSC-CMs, we inhibited α and β1 karyopherin activity using ivermectin and importazole, respectively. Like the effects observed in hiPSC-CMs, both ivermectin (2.5 μM) and importazole (40 μM) diminished nuclear targeting of the distal-CT and abolished nuclear targeting of the full-length-CT (Fig. 5). These data demonstrate that the hERG1 NLS drives nuclear transport of the distal-CT and full-length-CT polypeptides through the classical nuclear transport pathway, identical to the native $hERG1_{NP}$ in hiPSC-CMs.

The $hERG1_{NP}$ Inhibits I_{hERG1}. We used the distal-CT polypeptide as a tool to explore the functional impact of the $hERG1_{NP}$ on the electrophysiological properties of hERG1 currents. We transfected HEK293 cells stably expressing hERG1a with the distal-CT (Fig. 6). The distal-CT, acting as a surrogate of the native $hERG1_{NP}$, reduced tail current density by 55%, compared to GFP-transfected controls (Fig. 6 *A* and *B* and Table 1). The distal-CT reduced steady-state currents even further, by 78% compared to GFP controls (Fig. 6 *A* and *C* and Table 1). The equilibrium between the activated and inactivated states mediates

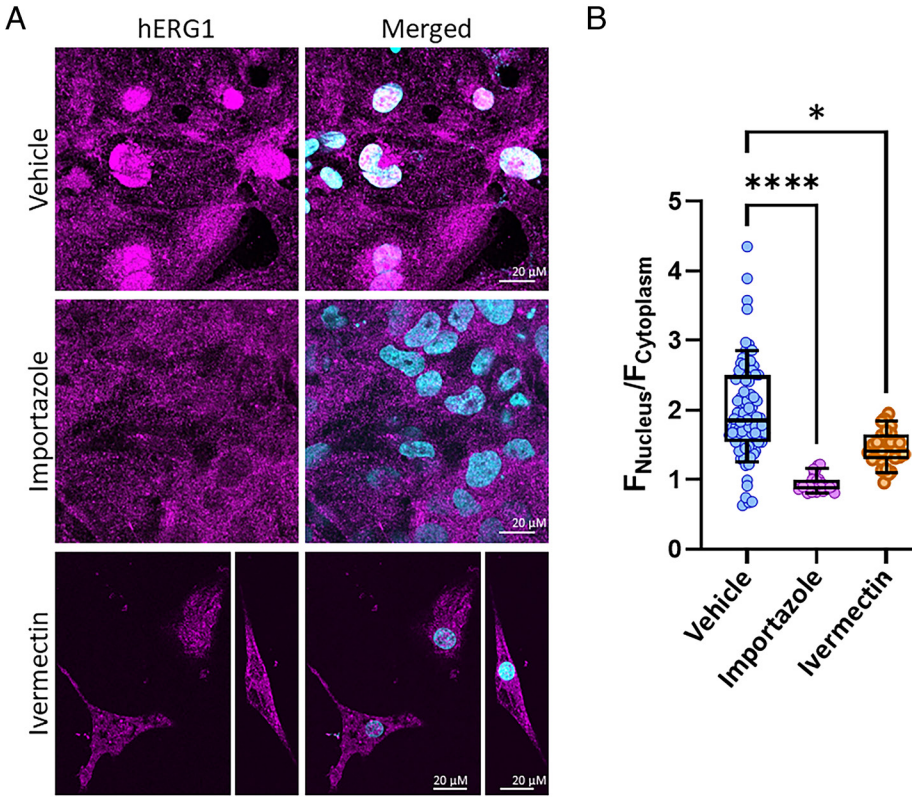

Fig. 3. The α/β_1 karyopherin complex regulates $hERG1_{NP}$ nuclear transport in hiPSC-CMs. (*A*) hiPSC-CMs following an 8hr incubation in either vehicle (*Top*), 40 μM importazole (*Middle*), or 2.5 μM ivermectin (*Bottom*), and stained for hERG1 with the C-Term antibody (*magenta*) and DAPI (*cyan*). (*B*) Box and whisker plots depicting nuclear fluorescence intensity relative to cytoplasmic fluorescence intensity ($F_{Nucleus}/F_{Cytoplasm}$) for the C-Term antibody. Importazole and ivermectin significantly reduced the nuclear enrichment of the C-Term antibody. Data were compared using a Kruskal–Wallis ANOVA. * indicates $P < 0.05$. **** indicates $P < 0.0001$

the magnitude of hERG steady-state current. We therefore hypothesized that the $hERG1_{NP}$ promotes hERG1 inactivation, thereby exacerbating steady-state current reduction compared to tail current reduction. To test this, we normalized steady-state currents to the maximum tail current recorded from the same cell to calculate the relative steady-state current—which is a proxy for the stability of the inactivated state. The distal-CT reduced the relative steady-state current magnitude from 1.00 ± 0.17 AU in the presence of GFP to 0.45 ± 0.06 AU in the presence of the $hERG1_{NP}$ (Table 1 and Fig. 6*D*). These data demonstrate that the distal-CT reduces hERG1 current by reducing channels at the membrane and by promoting inactivation.

We also measured the impact of the distal-CT on the time course of hERG1 deactivation. Distal-CT expression significantly slowed the time course of deactivation compared to GFP-transfected controls (Fig. 6 *E*–*G*). Given that the voltage dependence of activation was unaffected by the distal peptide (Table 1), these data also suggest that the distal peptide is similarly accelerating the time course of activation.

Finally, to evaluate if the effects of the distal-CT were dependent upon its targeting to inside the nucleus, we expressed the ΔNLS polypeptide. hERG1 currents recorded in the presence of the ΔNLS polypeptide were significantly larger compared to the distal-CT and similar to GFP controls (Fig. 6 *C*–*F*). These data demonstrate that the effects of the distal-CT are dependent upon its trafficking inside the nucleus. Together, these electrophysiological data demonstrate that nuclear targeting of the distal-CT dramatically but indirectly reduces hERG1 current magnitude, slows channel deactivation, and promotes hERG1 inactivation.

Discussion

Here we identified a *KCNH2*-encoded polypeptide, $hERG1_{NP}$, which is upregulated in immature cardiomyocytes. α and β1 karyopherins, in conjunction with a nuclear localization sequence in the distal hERG1 C-terminal domain, target $hERG1_{NP}$ to the nucleus. Nuclear targeting of the putative $hERG1_{NP}$ (the distal-CT) alters hERG1a gating and dramatically reduces hERG1a current magnitude. These data demonstrate that hERG1NP is a regulator of hERG1.

Our study identifies two mechanisms by which that nuclear targeting of the distal-CT polypeptide attenuates hERG1a currents. First, the reduced tail currents demonstrate that the distal-CT reduces hERG1a currents by attenuating hERG1a surface expression. Second, the reduced relative steady-state current demonstrates that altered gating also reduces current magnitude, likely through enhanced channel inactivation. Our data do not rule out the possibility that the distal-CT and/or the $hERG1_{NP}$ differentially regulates hERG1 subunits: hERG1a-1c and $hERG1_{USO}$. This is particularly relevant given the upregulation of the $hERG1_{NP}$ in immature myocytes and the dynamic nature of hERG1 subunit abundance in the developing myocardium (4, 47, 48) and heart failure (23). hERG1 variants are enriched in cases of sudden death in the young (6, 7), and $hERG1_{NP}$ dysfunction could be a contributing factor in these cases.

Our data likely rule out a downstream "cryptic" promoter and could also rule out IRES-mediated translation as drivers for $hERG1_{NP}$ expression. We generated the *KCNH2*-null stem cell line with a two base-pair insertion in exon 6 (hERG1a numbering), which fully abolished $hERG1_{NP}$ expression. Any promoters downstream of the

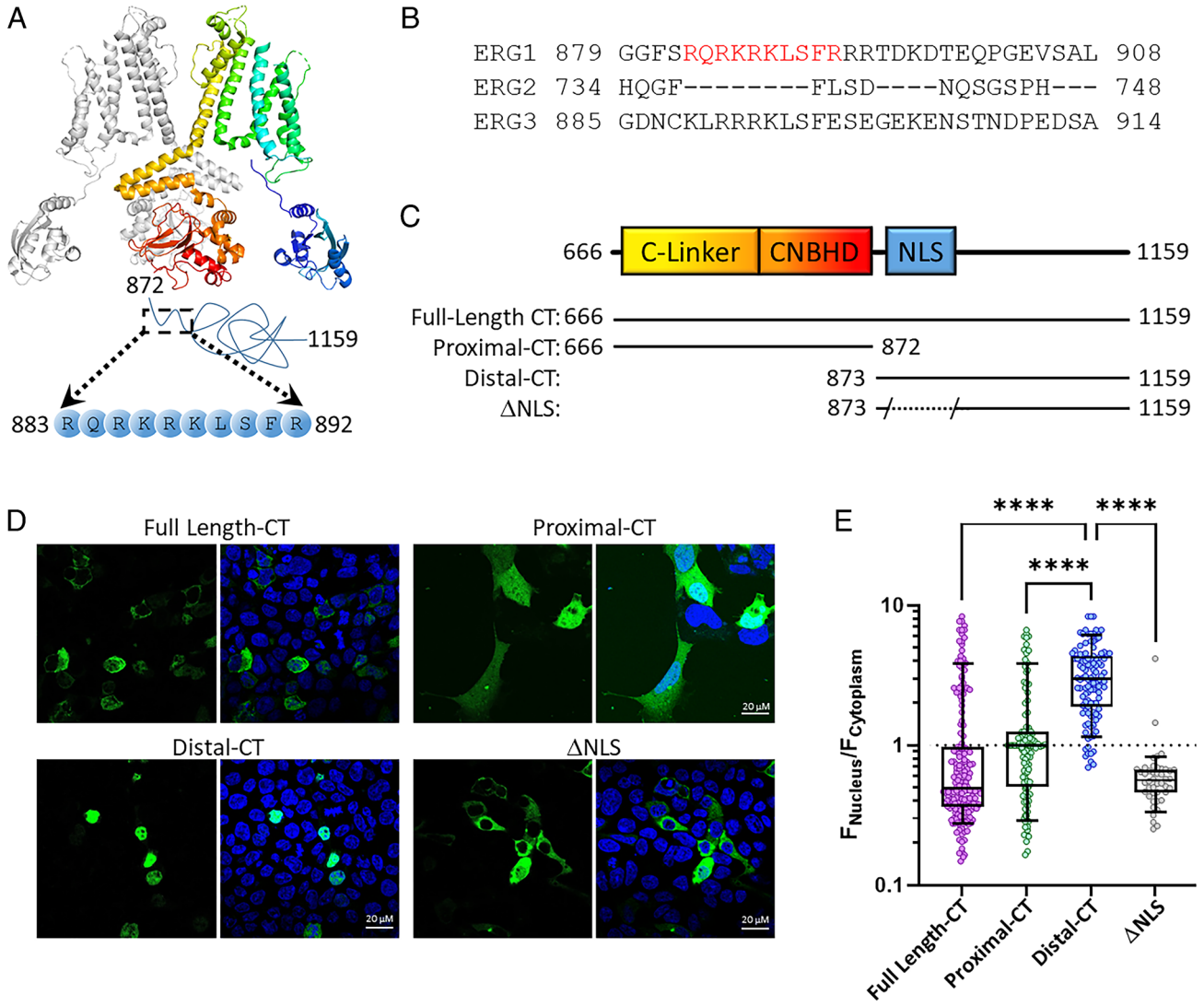

Fig. 4. A nuclear localization sequence in the distal C-terminal domain of hERG1. (*A*) Cryo-EM schematic depicting two opposing hERG1a subunits. The distal c-terminal domain with its NLS (883-892) is depicted with a blue line. (*B*) Amino acid sequence alignment of the ERG1 NLS with ERG2 and ERG3. (*C*) Schematic depicting the C-terminal coding regions of the full-length (666-1,159), proximal (666-872), distal (873-1,159), and ΔNLS constructs (873-882/893-1,159). (*D*) HEK293 cells expressing the full-length, proximal, distal, and ΔNLS constructs. (*E*) Box and whisker plots depicting the intracellular distribution of HEK293 cells transfected with the full-length (*magenta*), proximal (*green*), distal (*blue*), and ΔNLS (*gray*) constructs. Data were compared using a Kruskal–Wallis ANOVA. **** indicates $P < 0.0001$.

insertion would be predicted to remain functional. Although activity of a putative $hERG1_{NP}$ promoter could be tied to full-length hERG1 channel expression, this suggests that proteolytic cleavage of the full-length channel generates the $hERG1_{NP}$. And because the effects of the $hERG1_{NP}$ on channel gating were dependent upon nuclear targeting, these data suggest that the $hERG1_{NP}$ alters gene expression to indirectly modulate hERG1 channel function. Interestingly, deleting the distal hERG1 C-terminal domain does not impact hERG1a expression and minimally affects hERG1a channel gating (31, 32). These data suggest that generating the $hERG1_{NP}$ by proteolytic cleavage could occur with minimal effects on surface I_{Kr} gating.

Our data identify a *KCNH2*-encoded peptide that does not, at least directly, modulate hERG1 function. This adds to a growing body of work that highlights roles for *KCNH2* that are unrelated to cardiac repolarization. Recent work in rat cells demonstrated that rERG1 complexes with integrin β1 to activate FAK signaling during cardiac differentiation and cardiac recovery following sepsis (49, 50). hERG1 displays a similar role in cancer lines, where hERG1 promotes proliferation and metastasis (51, 52). Our data are interesting because $hERG1_{NP}$ expression diminished sharply with cardiomyocyte maturation, which roughly corresponds with the transition from hyperplasia (embryonic & fetal cardiomyocytes) to hypertrophy (neonatal & adult cardiomyocytes) (53). This suggests a potential role for the $hERG1_{NP}$ in developing cardiomyocyte division and/or proliferation. Indeed, the full-length C-terminus displayed a bimodal distribution (nuclear vs cytoplasmic targeting, c.f. Fig. 4). These HEK293 data also support cell-cycle activity as a factor in $hERG1_{NP}$ nuclear targeting.

hERG1's widespread expression and association with diseases across multiple organs and tissues point to a fundamental role for *KCNH2* in human physiology. hERG1 is widely expressed in the brain, and its dysfunction is associated with schizophrenia (54, 55) and epilepsy (56, 57). Pancreatic beta cells express *KCNH2*, and loss-of-function *KCNH2* variants are associated with hyperinsulinemia and diabetes (58, 59). KCNH2 is also expressed in smooth muscle tissues, where it regulates contractile function (60, 61), and is associated with vascular remodeling (62, 63).

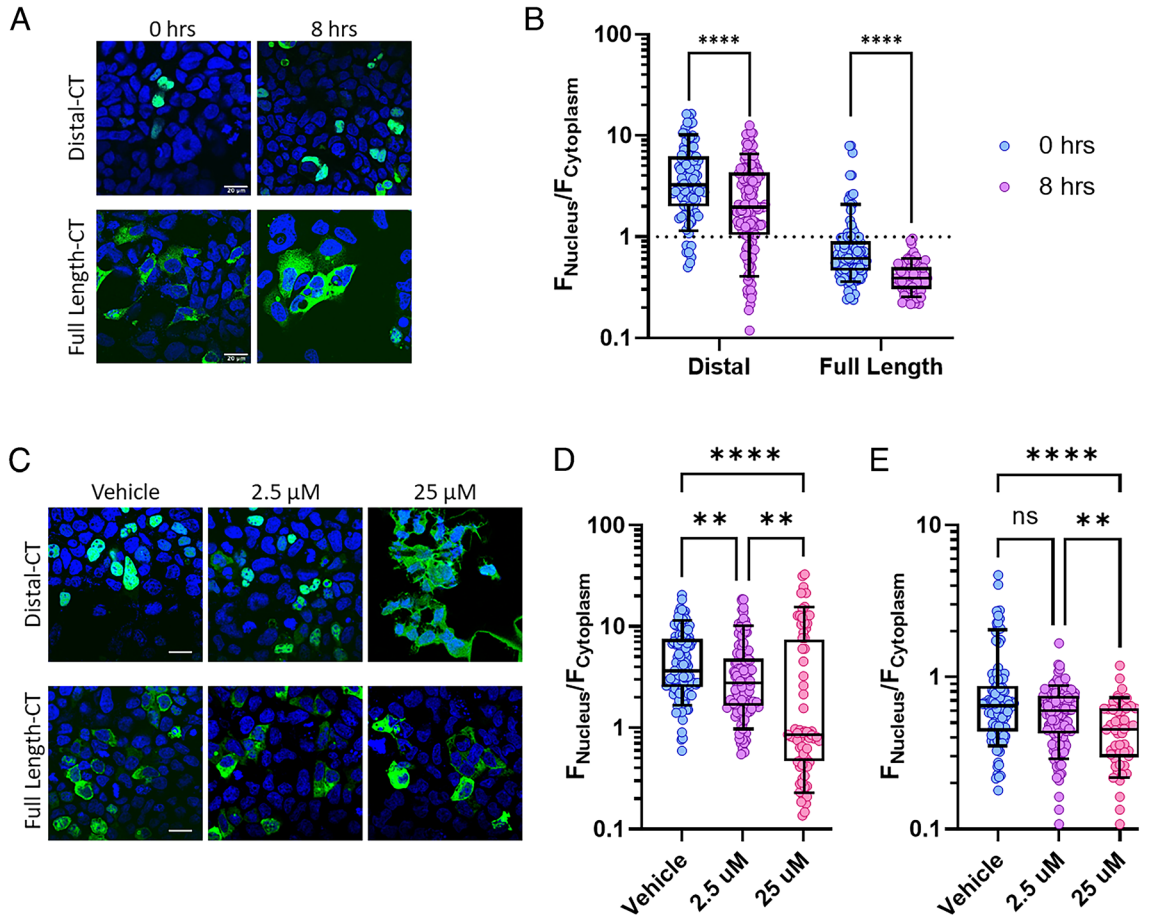

Fig. 5. The α/β_1 karyopherin complex regulates nuclear targeting of hERG1 C-terminal truncates. (*A*) HEK293 cells expressing the distal (*Top*) and full-length (*Bottom*) peptides (*green*) at 0 and 8 hrs, with 40 µM importazole. (*B*) Box and whisker plots depicting intracellular distribution of the full-length and distal peptides before and after 8 h incubation with 40 µM importazole. (*C*) HEK293 cells expressing the distal (*Top*) and full-length (*Bottom*) peptides incubated in vehicle, 2.5 µM ivermectin, or 25 µM ivermectin for 4 h. (*D* and *E*) Box and whisker plots depicting intracellular distribution of the distal (*D*) and full-length (*E*) peptides before and after as in "*C*." Data in "*B*" were compared using a Mann–Whitney test. Data in "*D*" and "*E*" were compared using a Kruskal–Wallis ANOVA. * $P < 0.05$. indicates, ** indicates $P < 0.01$. ** indicates $P < 0.01$. **** indicates $P < 0.0001$.

The integral role of ERG1 is best highlighted by work in mice. I_{Kr} minimally regulates adult murine cardiac excitability, yet loss of *KCNH2* expression is embryonically lethal, triggering a myriad of morphological cardiac defects (64–66). *KCNH2* transcripts are observed at the earliest stages of mouse cardiac development (67) and have even been reported in developing mouse embryos prior to implantation (68). In fact, loss-of-function *KCNH2* variants have been identified in cases of tetralogy de Fallot (69, 70), which suggests that hERG1 may also contribute to cardiomorphogenesis in humans as well. Evolutionary analysis also demonstrates an ancestral origin for ERG channels that predates the divergence of cnidarians and bilaterians (71). With such an ancient origin, it is rational to presume that hERG1 function is integrated in widespread aspects of physiology. The identification of $hERG1_{NP}$ represents one step closer to understanding the breadth of mechanisms by which *KCNH2* regulates human physiology.

Finally, hERG1 is not the ion channel-related peptide to display a nuclear-targeted subdomain. Proteins encoded by *GJA1* (Cx43), *CACNA1A* ($Ca_V2.1$), *CACNA1C* ($Ca_V1.2$), *TRPM7* (TRPM7), and *SCN1B* (Na_V channel β_1 subunit) display similar activity (72–75). These peptides are generated by either proteolytic cleavage (72, 76–78) or alternative forms of translation such as a cryptic promoter or internal ribosomal entry site (73, 74, 79, 80). For example, mRNA of the *CACNA1C* gene encodes the full-length channel, $Ca_V1.2$, and a smaller, 75 kDa transcription factor called CCAT (73, 79). CCAT is identical to the C-terminus of $Ca_V1.2$ but is targeted to the nucleus where it regulates expression of neuronal signaling genes (73, 79). Similarly in *CACNA1A*, an internal ribosomal entry site (IRES) initiates translation of a transcription factor called α1ACT, which promotes neural and Purkinje cell development (74). The TRPM7 displays tissue-specific proteolytic cleavage. Similar to *KCNH2*, TRPM7 displays low-level expression throughout the body, yet its disruption is embryonically lethal (72). The cleaved TRPM7 polypeptides phosphorylate core histones leading to altered gene expression that is necessary for embryonic development (81). Nuclear trafficking of these ion channel subdomains appears to function as an additional feedback mechanism between activity at the surface membrane and gene expression within the nucleus (73, 75, 79, 82). This growing body of research demonstrates that the roles of ion channel proteins limit aspect of cellular physiology beyond membrane potential.

Materials and Methods

CRISPR *KCNH2* Deletion. *KCNH2* deletion was completed by CRISPR by the University of Michigan Stem Cell and Gene Editing Core in the H9 human embryonic stem cell background. H9 cells were obtained from the WiCell stem cell repository. The gene-editing core generated a guide RNA (gRNA) targeting *KCNH2*-exon 6 using the CRIPSR design tool *via* the UCSC genome browser

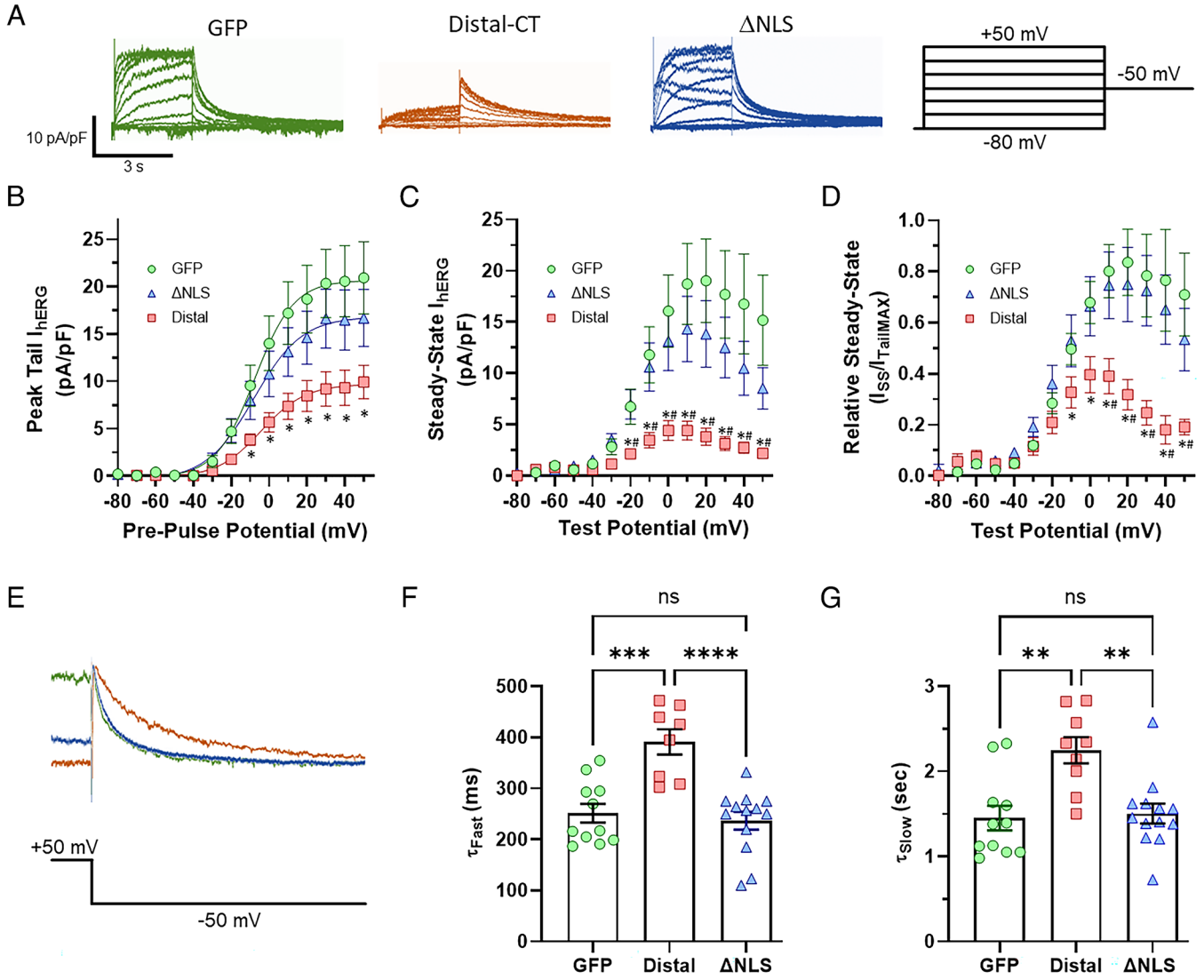

Fig. 6. The hERG1$_{NP}$ inhibits I_{hERG1}. (*A*) Sample current traces recorded from HEK293 cells stably expressing hERG1a and transfected with vectors encoding either GFP (*green*), Distal (*red*), or ΔNLS constructs (*blue*). Voltage protocol used is shown at right. (*B*) Peak tail current density (pA/pF) plotted as a function of pre-pulse potential and fitted with a Boltzmann function, recorded from HEK293 cells stably expressing hERG1a and transfected with GFP (*green circles*), Distal (*red squares*), or ΔNLS (*blue triangles*). The Distal peptide significantly reduced tail current density compared to GFP and ΔNLS. (*C*) Steady-state current density (pA/pF) plotted as a function of test potential for GFP (*green circles*), Distal (*red squares*), or ΔNLS (*blue triangles*). The Distal peptide significantly reduced steady-state current density compared to GFP and ΔNLS. (*D*) Relative steady-state current magnitude ($I_{SS}/I_{TailMAX}$) plotted as a function of test potential for GFP (*green circles*), Distal (*red squares*), or ΔNLS (*blue triangles*). The Distal peptide significantly reduced relative steady-state current density compared to GFP and ΔNLS. n = 9 to 12. * indicates $P < 0.05$ vs GFP. # indicates $P < 0.05$ vs ΔNLS. (*E*) Sample traces depicting deactivation from GFP (*green*), Distal (*blue*), and ΔNLS (*red*). The distal peptide significantly slowed the time course of deactivation compared to GFP or ΔNLS. (*F*) Fast time constants of deactivation for GFP (*green circles*), Distal (*red squares*), and ΔNLS (*blue triangles*). (*G*) Slow time constants of deactivation for GFP, Distal, and ΔNLS. Data in "*B–D*" were compared using a two-way ANOVA. Data in "*F* and "*G*" were compared using a one-way ANOVA. ** indicates $P < 0.01$. *** indicates $P < 0.001$. **** indicates $P < 0.0001$.

on the human GRCh38/hg38 assembly (https://genome.ucsc.edu/), sgRNA1: ATGAGGTCCACCACAGCCAGCGG, sgRNA2: CTCCTCGTTGGCATTGACGTAGG. We verified a two base-pair deletion in exon 6 by Sanger sequencing using the forward and reverse primers TCCTCTCCCTACACCACCTG and CTCCTCCTCATTCTGCTTGG, respectively (*SI Appendix*, Fig. S1). Isogenic control and gene-edited *KCNH2*-null hESCs displayed appropriate pluripotency markers and differentiated into contracting hESC-CMs (Fig. 2 and *SI Appendix*, Fig. S1).

Stem Cell Culture and Cardiac Differentiation. We cultured and differentiated human iPS (df19.9.11, WiCell) and ES (H9, WiCell) cells into cardiomyocytes using the GiWi protocol, as described (42). Briefly, we seeded stem cells on Matrigel-coated plasticware with iPS-brew medium. We checked media daily to remove spontaneous differentiation and passed the cells at 70% confluence. At the day of cell passage, we re-seeded cells to continue the line, or seeded the cells to grow monolayers for cardiac-directed differentiation. We plated 4 × 10^5 cells into each well of a 6-well plate and cultured them to ~80% confluence for treatment with GSK3 inhibitor for induction of mesodermal differentiation (day 0, D0). Following mesodermal differentiation, we treated cells with a Wnt inhibitor for induction of cardiac mesoderm (D2). On D4, we removed Wnt inhibition to direct the cells into cardiac progenitor cells. Cardiomyocytes with autonomous contractility emerged 8 to 10 d after initiation of cardiac-directed differentiation. We cultured the cardiomyocytes until 20 d after initiation of differentiation, and isolated purified cardiomyocytes by magnetic-beads assisted isolation with an iPSC-Derived Cardiomyocyte Isolation Kit, human (Miltenyi Biotec, USA) following the manufacturer's recommendations. We plated the purified cardiomyocytes on Matrigel-coated coverslips for 7 d before completing experiments.

HEK293 Cell Culture. We maintained all cells at 37 °C and 5% CO_2 in a Heracell incubator (Thermo Fisher). We cultured HEK293 cells in minimum essential medium (MEM, Invitrogen, Cat. No. 11095080) supplemented with 10% fetal bovine serum (Thermo Fisher, Cat. No. SH30070.03) and split every 3 to 5 d at 60 to 80% confluency.

Table 1. Electrophysiological parameters of I_{hERG} in HEK293 cells

	Electrophysiological parameters of I_{hERG}					
	$V_{1/2}$ (mV)	k	I_{tail} Max (pA/pF)	I_{ss} Max (pA/pF)	Relative I_{SS}	n
GFP	−6.2 ± 2.0	10.0 ± 0.4	21.4 ± 3.8	23.0 ± 5.2	1.00 ± 0.17	11
Distal	−5.3 ± 1.7	11.0 ± 1.0	9.6 ± 1.9*	4.9 ± 1.0*,†	0.45 ± 0.06*,†	10
ΔNLS	−10.7 ± 2.8	11.3 ± 0.8	17.5 ± 3.3	15.7 ± 3.2	0.86 ± 0.13	11

*Indicates statistically significant compared to GFP.
†Indicates statistically significant compared to ΔNLS.

Stem Cell-derived Cardiomyocyte Electrophysiology. We completed all recordings at physiological temperature (37 ± 1 °C) using whole-cell patch clamp with an IPA running and Sutterpatch (Sutter). We performed leak subtraction off-line based on measured current observed at potentials negative to I_{Kr} activation. The inter-pulse duration for all recordings was 10 s.

We sampled data at 10 kHz and low-pass filtered at 1 kHz. Cells were perfused with extracellular solution containing (in mM): 150 NaCl, 5.4 KCl, 1.8 $CaCl_2$, 1 $MgCl_2$, 15 glucose, 10 HEPES, 1 Na-pyruvate, and titrated to pH 7.4 using NaOH. Recording pipettes had resistances of 2 to 4.5 MW when backfilled with intracellular solution containing (in mM): 5 NaCl, 150 KCl, 2 $CaCl_2$, 5 EGTA, 10 HEPES, 5 MgATP, and titrated to pH 7.2 using KOH. We isolated I_{Kr} as an E-4031-sensitive current, as described (19, 35, 83). We preceded I_{Kr} recordings with a 100 ms step to −40 mV to inactivate the voltage-gated sodium currents. To elicit I_{Kr}, we stepped from the −40 mV pre-pulse to membrane potentials between −50 mV and +60 mV in 10 mV increments. We measured tail currents during a −40 mV, 3-s test pulse. To describe the voltage dependence of I_{Kr} activation, we normalized peak tail current to cellular capacitance, plotted current density as a function of pre-pulse potential, and fitted the data with the following Boltzmann equation:

$$y = \left[\frac{A_1 - A_2}{1 + e^{(V - V_0)/k}}\right] + A_2, \qquad [1]$$

where A_1 and A_2 represent the maximum and minimums of the fit, respectively, V is the membrane potential, V_0 is the midpoint, and k is the slope factor.

HEK293 Electrophysiology. We completed all HEK293 recordings identical to cardiomyocyte recordings with the following exceptions. We completed HEK293 recordings at room temperature. We completed leak subtraction off-line at potentials −80 mV. To elicit I_{hERG1}, we stepped from −80 mV to membrane potentials between −80 mV and +50 mV in 10 mV increments. We measured tail currents during a −50 mV, 3-s test pulse. To describe the voltage dependence of I_{hERG1} activation, we normalized peak tail current to cellular capacitance, plotted current density as a function of pre-pulse potential, and fitted the data with a Boltzmann equation (Eq. 1). To measure the time course of deactivation, we fit current decay during a −50 mV test pulse from +30 mV with a double exponential function:

$$y = Y_0 + A_1 e^{-t/\tau_1} + A_2 e^{-t/\tau_2}, \qquad [2]$$

where Y_0 is the asymptote, A_1 and A_2 represent the maximum and minimums the fast and slow time constants (τ_1 and τ_2), respectively.

Stem Cell-Derived and Native Cardiomyocyte Immunocytochemistry. We validated the differentiated cardiac lines using immunocytochemistry targeting actin (phalloidin, cat #A12379 ThermoFisher) to display the cardiac sarcomere organization, and patch clamp electrophysiology measuring cardiac I_{Kr}, indicative of hERG1 expression. To target the hERG1 p-loop, we immunolabeled all cardiomyocytes with 1:200 dilution of primary antibody #ALX-804-652-R300 from Enzo Life Sciences and 1:250 dilution of secondary antibody goat anti-mouse Alexa Fluor 568 (#A-11004, Invitrogen). To target the hERG1 C-terminal domain, we immunolabeled cardiomyocytes with a 1:150 dilution of primary antibody #ALX-215-049-R100 from Enzo Life Sciences and 1:250 dilution of secondary antibody AF647, Goat Anti-Rabbit, Cat. #4050-31 from Southern Biotech. We labeled the nuclei using 1:1,000 dilution of DAPI (1 μg/mL) for 15 min (ThermoScientific, Cat. #62248).

HEK293 Cell Immunocytochemistry. We cultured cells to 60% confluency in 6-well plastic dishes. We transfected cells with 1 μg DNA using Lipofectamine 3000. 24 h after transfection, we replated cells onto 12 mm No. 1.5 glass coverslips. 48 h after transfection, we fixed cells using 4% pfa for 15 min. We washed the fixed cells three times using PBS and stained using DAPI at (1 μg/mL) for 15 min and then washed three more times with PBS. We mounted the coverslips on microscope slides using Prolong Gold mounting medium and completed imaging 48 h after mounting. We completed all imaging using a Zeiss 880 confocal microscope.

DNA Constructs. The hERG1 proximal domain (666-872-Citrine.pcDNA3), distal domain (873-1,159-Citrine.pcDNA3), and full-length C-terminal domain (666-1,159-Citrine.pcDNA3) plasmids were generously provided by Professor Matthew Trudeau at the University of Maryland Medical School. We generated the 873-1,159-Citrine ΔNLS mutant using site-directed mutagenesis (QuikChange II Kit, Agilent Technologies) using the distal plasmid as a template. We designed the primers (Forward, 5′-ccgtgcgcctactgaagccaccctctaac-3′: Reverse, 5′-gttagaggtggcttcagtaggcgcacgg-3′) with the QuikChange Primer Design (agilent.com), and the primers were synthesized by Eurofins. We verified the sequences of all constructs by DNA sequencing (Eurofins).

Statistical Analysis. We completed analysis using IgorPro and Prism (Graphpad). We evaluated values for normality with a Shapiro-Wilk test, which determined the use of either a parametric (i.e., Student's) or non-parametric (i.e., Mann–Whitney) tests to calculate statistical significance between groups. One-way or two-way ANOVA, with a Bonferroni *post hoc t* tests were also implemented, where appropriate. Specific tests for each comparison are described in the figure legends. We also evaluated for outliers (ROUT and Grubbs' test) before statistical evaluation. All data are reported as mean ± SEM. Statistical significance was taken at $P < 0.05$.

Data, Materials, and Software Availability. All study data are included in the article and/or *SI Appendix*.

ACKNOWLEDGMENTS. This work was supported by R00HL133482 and a Samuel and Jean Frankel Cardiovascular Center Amplifier Grant to D.K.J., T32-GM140223 to F.G.S.-C., T32-GM007767 to C.U.U., and T32-HL125242 to C.U.U. The authors thank the University of Michigan Gene Editing Core for generating the *KCNH2*-null human embryonic stem cell line, and Matt C. Trudeau for providing the hERG1 C-terminal constructs.

1. M. C. Trudeau, J. W. Warmke, B. Ganetzky, G. A. Robertson, HERG, a human inward rectifier in the voltage-gated potassium channel family. *Science* **269**, 92–95 (1995).
2. M. C. Sanguinetti, C. Jiang, M. E. Curran, M. T. Keating, A mechanistic link between an inherited and an acquired cardiac arrhythmia: HERG encodes the IKr potassium channel. *Cell* **81**, 299–307 (1995).
3. M. E. Curran *et al.*, A molecular basis for cardiac arrhythmia: HERG mutations cause long QT syndrome. *Cell* **80**, 795–803 (1995).
4. L. Crotti *et al.*, Long QT syndrome-associated mutations in intrauterine fetal death. *Jama* **309**, 1473–1482 (2013).
5. T. E. Rhodes *et al.*, Cardiac potassium channel dysfunction in sudden infant death syndrome. *J. Mol. Cell Cardiol.* **44**, 571–581 (2008).
6. M. Arnestad *et al.*, Prevalence of long-QT syndrome gene variants in sudden infant death syndrome. *Circulation* **115**, 361–367 (2007).

7. M. S. Soh *et al.*, Loss-of-function variants in Kv 11.1 cardiac channels as a biomarker for SUDEP. *Ann. Clin. Transl. Neurol.* **8**, 1422–1432 (2021).
8. R. D. Bagnall *et al.*, A prospective study of sudden cardiac death among children and young adults. *N. Engl. J. Med.* **374**, 2441–2452 (2016).
9. E. Tu, R. D. Bagnall, J. Duflou, C. Semsarian, Post-mortem review and genetic analysis of sudden unexpected death in epilepsy (SUDEP) cases. *Brain Pathol.* **21**, 201–208 (2011).
10. B. London *et al.*, Two isoforms of the mouse ether-a-go-go-related gene coassemble to form channels with properties similar to the rapidly activating component of the cardiac delayed rectifier K+ current. *Circ. Res.* **81**, 870–878 (1997).
11. J. P. Lees-Miller, C. Kondo, L. Wang, H. J. Duff, Electrophysiological characterization of an alternatively processed ERG K+ channel in mouse and human hearts. *Circ. Res.* **81**, 719–726 (1997).
12. S. Kupershmidt, D. J. Snyders, A. Raes, D. M. Roden, A K+ channel splice variant common in human heart lacks a C-terminal domain required for expression of rapidly activating delayed rectifier current. *J. Biol. Chem.* **273**, 27231–27235 (1998).
13. E. C. Gianulis, Q. Liu, M. C. Trudeau, Direct interaction of eag domains and cyclic nucleotide-binding homology domains regulate deactivation gating in hERG channels. *J. Gen. Physiol.* **142**, 351–366 (2013).
14. A. S. Gustina, M. C. Trudeau, The eag domain regulates hERG channel inactivation gating via a direct interaction. *J. Gen. Physiol.* **141**, 229–241 (2013).
15. C. A. Ng, K. Phan, A. P. Hill, J. I. Vandenberg, M. D. Perry, Multiple interactions between cytoplasmic domains regulate slow deactivation of Kv11.1 channels. *J. Biol. Chem.* **289**, 25822–25832 (2014).
16. C. A. Harley *et al.*, Conformation-sensitive antibody reveals an altered cytosolic PAS/CNBh assembly during hERG channel gating. *Proc. Natl. Acad. Sci. U.S.A.* **118**, e2108796118 (2021).
17. J. H. Morais Cabral *et al.*, Crystal structure and functional analysis of the HERG potassium channel N terminus: A eukaryotic PAS domain. *Cell* **95**, 649–655 (1998).
18. H. Sale *et al.*, Physiological properties of hERG 1a/1b heteromeric currents and a hERG 1b-specific mutation associated with Long-QT syndrome. *Circ. Res.* **103**, e81–95 (2008).
19. D. K. Jones *et al.*, hERG 1b is critical for human cardiac repolarization. *Proc. Natl. Acad. Sci. U.S.A.* **111**, 18073–18077 (2014).
20. C. A. Harley *et al.*, Enhancement of hERG channel activity by scFv antibody fragments targeted to the PAS domain. *Proc. Natl. Acad. Sci. U.S.A.* **113**, 9916–9921 (2016).
21. L. Guasti *et al.*, Identification of a posttranslational mechanism for the regulation of hERG1 K+ channel expression and hERG1 current density in tumor cells. *Mol. Cell Biol.* **28**, 5043–5060 (2008).
22. Q. Gong, M. R. Stump, A. R. Dunn, V. Deng, Z. Zhou, Alternative splicing and polyadenylation contribute to the generation of hERG1 C-terminal isoforms. *J. Biol. Chem.* **285**, 32233–32241 (2010).
23. K. M. Holzem *et al.*, Reduced response to IKr blockade and altered hERG1a/1b stoichiometry in human heart failure. *J. Mol. Cell Cardiol.* **96**, 82–92 (2016).
24. S. J. Codding, M. C. Trudeau, The hERG potassium channel intrinsic ligand regulates N- and C-terminal interactions and channel closure. *J. Gen. Physiol.* **151**, 478–488 (2019).
25. Y. Haitin, A. E. Carlson, W. N. Zagotta, The structural mechanism of KCNH-channel regulation by the eag domain. *Nature* **501**, 444–448 (2013).
26. T. I. Brelidze, A. E. Carlson, B. Sankaran, W. N. Zagotta, Structure of the carboxy-terminal region of a KCNH channel. *Nature* **481**, 530–533 (2012).
27. C. M. Hull, S. Sokolov, A. C. Van Slyke, T. W. Claydon, Regional flexibility in the S4–S5 linker regulates hERG channel closed-state stabilization. *Pflugers Arch.* **466**, 1911–1919 (2014).
28. J. Wang, C. D. Myers, G. A. Robertson, Dynamic control of deactivation gating by a soluble amino-terminal domain in HERG K(+) channels. *J. Gen. Physiol.* **115**, 749–758 (2000).
29. J. Wang, M. C. Trudeau, A. M. Zappia, G. A. Robertson, Regulation of deactivation by an amino terminal domain in human ether-a- go-go-related gene potassium channels. *J. Gen. Physiol.* **112**, 637–647 (1998).
30. C. L. Anderson *et al.*, Large-scale mutational analysis of Kv11.1 reveals molecular insights into type 2 long QT syndrome. *Nat. Commun.* **5**, 5535 (2014).
31. W. Wang, R. MacKinnon, Cryo-EM structure of the open human ether-a-go-go-related K(+) Channel hERG. *Cell* **169**, 422–430.e410 (2017).
32. T. Asai *et al.*, Cryo-EM structure of K(+)-bound hERG channel complexed with the blocker astemizole. *Structure* **29**, 203–212 e204 (2021).
33. J. L. Smith *et al.*, Functional invalidation of putative sudden infant death syndrome-associated variants in the KCNH2-encoded Kv11.1 channel. *Circ. Arrhythm. Electrophysiol.* **11**, e005859 (2018).
34. Y. Guo, W. T. Pu, Cardiomyocyte maturation: New phase in development. *Circ. Res.* **126**, 1086–1106 (2020).
35. D. K. Jones *et al.*, Localization and functional consequences of a direct interaction between TRIOBP-1 and hERG proteins in the heart. *J. Cell Sci.* **131**, jcs206730 (2018).
36. J. Ma *et al.*, High purity human-induced pluripotent stem cell-derived cardiomyocytes: electrophysiological properties of action potentials and ionic currents. *Am. J. Physiol. Heart Circ. Physiol.* **301**, H2006–2017 (2011).
37. E. Matsa *et al.*, Drug evaluation in cardiomyocytes derived from human induced pluripotent stem cells carrying a long QT syndrome type 2 mutation. *Eur. Heart J.* **32**, 952–962 (2011).
38. I. Itzhaki *et al.*, Modelling the long QT syndrome with induced pluripotent stem cells. *Nature* **471**, 225–229 (2011).
39. A. Moretti *et al.*, Patient-specific induced pluripotent stem-cell models for long-QT syndrome. *N. Engl. J. Med.* **363**, 1397–1409 (2010).
40. J. Zhang *et al.*, Extracellular matrix promotes highly efficient cardiac differentiation of human pluripotent stem cells: The matrix sandwich method. *Circ. Res.* **111**, 1125–1136 (2012).
41. C. Mummery *et al.*, Differentiation of human embryonic stem cells to cardiomyocytes: Role of coculture with visceral endoderm-like cells. *Circulation* **107**, 2733–2740 (2003).
42. T. Block *et al.*, Human perinatal stem cell derived extracellular matrix enables rapid maturation of hiPSC-CM structural and functional phenotypes. *Sci. Rep.* **10**, 19071 (2020).
43. D. Görlich *et al.*, Two different subunits of importin cooperate to recognize nuclear localization signals and bind them to the nuclear envelope. *Curr. Biol.* **5**, 383–392 (1995).
44. K. M. Wagstaff, H. Sivakumaran, S. M. Heaton, D. Harrich, D. A. Jans, Ivermectin is a specific inhibitor of importin α/β-mediated nuclear import able to inhibit replication of HIV-1 and dengue virus. *Biochem. J.* **443**, 851–856 (2012).
45. J. F. Soderholm *et al.*, Importazole, a small molecule inhibitor of the transport receptor importin-β. *ACS Chem. Biol.* **6**, 700–708 (2011).
46. M. Christie *et al.*, Structural biology and regulation of protein import into the nucleus. *J. Mol. Biol.* **428**, 2060–2090 (2016).
47. J. P. Lees-Miller *et al.*, Selective knockout of mouse ERG1 B potassium channel eliminates I(Kr) in adult ventricular myocytes and elicits episodes of abrupt sinus bradycardia. *Mol. Cell Biol.* **23**, 1856–1862 (2003).
48. X. Wang *et al.*, Kv11.1 channel subunit composition includes MinK and varies developmentally in mouse cardiac muscle. *Dev. Dyn.* **237**, 2430–2437 (2008).
49. Z. Li *et al.*, Kcnh2 mediates FAK/AKT-FOXO3A pathway to attenuate sepsis-induced cardiac dysfunction. *Cell Prolif* **54**, e12962 (2021).
50. D. Wang *et al.*, ERG1 plays an essential role in rat cardiomyocyte fate decision by mediating AKT signaling. *Stem. cells* **39**, 443–457 (2021).
51. A. Cherubini *et al.*, Human ether-a-go-go-related gene 1 channels are physically linked to beta1 integrins and modulate adhesion-dependent signaling. *Mol. Biol. Cell* **16**, 2972–2983 (2005).
52. A. Becchetti *et al.*, The conformational state of hERG1 channels determines integrin association, downstream signaling, and cancer progression. *Sci. Signal* **10**, eaaf3236 (2017).
53. F. Li, X. Wang, J. M. Capasso, A. M. Gerdes, Rapid transition of cardiac myocytes from hyperplasia to hypertrophy during postnatal development. *J. Mol. Cell Cardiol.* **28**, 1737–1746 (1996).
54. S. J. Huffaker *et al.*, A primate-specific, brain isoform of KCNH2 affects cortical physiology, cognition, neuronal repolarization and risk of schizophrenia. *Nat. Med.* **15**, 509–518 (2009).
55. F. Atalar *et al.*, Two four-marker haplotypes on 7q36.1 region indicate that the potassium channel gene HERG1 (KCNH2, Kv11.1) is related to schizophrenia: A case control study. *Behav. Brain Funct.* **6**, 27 (2010).
56. D. S. Auerbach *et al.*, Genetic biomarkers for the risk of seizures in long QT syndrome. *Neurology* **87**, 1660–1668 (2016).
57. J. N. Johnson *et al.*, Identification of a possible pathogenic link between congenital long QT syndrome and epilepsy. *Neurology* **72**, 224–231 (2009).
58. A. F. Lubberding *et al.*, Celebrities in the heart, strangers in the pancreatic beta cell: Voltage-gated potassium channels K(v) 7.1 and K(v) 11.1 bridge long QT syndrome with hyperinsulinaemia as well as type 2 diabetes. *Acta Physiol. (Oxf)* **234**, e13781 (2022).
59. B. Rosati *et al.*, Glucose- and arginine-induced insulin secretion by human pancreatic beta-cells: The role of HERG K(+) channels in firing and release. *Faseb. J.* **14**, 2601–2610 (2000).
60. A. M. Farrelly *et al.*, Expression and function of KCNH2 (HERG) in the human jejunum. *Am. J. Physiol. Gastrointest Liver Physiol.* **284**, G883–895 (2003).
61. S. Ohya, K. Asakura, K. Muraki, M. Watanabe, Y. Imaizumi, Molecular and functional characterization of ERG, KCNQ, and KCNE subtypes in rat stomach smooth muscle. *Am. J. Physiol. Gastrointest Liver Physiol.* **282**, G277–287 (2002).
62. S. G. Gychka *et al.*, Placental vascular remodeling in pregnant women with COVID-19. *PloS one* **17**, e0268591 (2022).
63. N. V. Shults, V. Rybka, Y. J. Suzuki, T. I. Brelidze, Increased smooth muscle Kv11.1 channel expression in pulmonary hypertension and protective role of Kv11.1 channel blocker dofetilide. *Am. J. Pathol.* **190**, 48–56 (2020).
64. G. Salama, L. Baker, R. Wolk, J. Barhanin, B. London, Arrhythmia phenotype in mouse models of human long QT. *J. Interv. Card Electrophysiol.* **24**, 77–87 (2009).
65. G. Q. Teng *et al.*, Homozygous missense N629D hERG (KCNH2) potassium channel mutation causes developmental defects in the right ventricle and its outflow tract and embryonic lethality. *Circ. Res.* **103**, 1483–1491 (2008).
66. G. Teng *et al.*, Role of mutation and pharmacologic block of human KCNH2 in vasculogenesis and fetal mortality: Partial rescue by transforming growth factor-beta. *Circ. Arrhythm. Electrophysiol.* **8**, 420–428 (2015).
67. D. Franco *et al.*, Divergent expression of delayed rectifier K(+) channel subunits during mouse heart development. *Cardiovasc. Res.* **52**, 65–75 (2001).
68. N. J. Winston, M. H. Johnson, J. M. McConnell, D. I. Cook, M. L. Day, Expression and role of the ether-à-go-go-related (MERG1A) potassium-channel protein during preimplantation mouse development. *Biol. Reprod.* **70**, 1070–1079 (2004).
69. J. Zhuang *et al.*, Case report: Prenatal whole-exome sequencing identified a novel nonsense mutation of the KCNH2 gene in a fetus with familial 2q14.2 duplication. *Front. Genet.* **13**, 924573 (2022).
70. Z. A. Bhuiyan *et al.*, Not all pathogenic mutations are pathogenic: KCNH2 mutations in two sisters with tetralogy of Fallot. *Int. J. Cardiol.* **172**, 276–277 (2014).
71. A. S. Martinson *et al.*, Functional evolution of Erg potassium channel gating reveals an ancient origin for IKr. *Proc. Natl. Acad. Sci. U.S.A.* **111**, 5712–5717 (2014).
72. J. Jin *et al.*, The channel kinase, TRPM7, is required for early embryonic development. *Proc. Natl. Acad. Sci. U.S.A.* **109**, E225–233 (2012).
73. N. Gomez-Ospina, F. Tsuruta, O. Barreto-Chang, L. Hu, R. Dolmetsch, The C terminus of the L-type voltage-gated calcium channel Ca(V)1.2 encodes a transcription factor. *Cell* **127**, 591–606 (2006).
74. X. Du *et al.*, Second cistron in CACNA1A gene encodes a transcription factor mediating cerebellar development and SCA6. *Cell* **154**, 118–133 (2013).
75. I. Epifantseva *et al.*, An alternatively translated connexin 43 isoform, GJA1-11k, localizes to the nucleus and can inhibit cell cycle progression. *Biomolecules* **10**, 473 (2020).
76. J. P. Bannister *et al.*, The voltage-dependent L-type Ca2+ (CaV1.2) channel C-terminus fragment is a bi-modal vasodilator. *J. Physiol.* **591**, 2987–2998 (2013).
77. H. K. Wong *et al.*, beta Subunits of voltage-gated sodium channels are novel substrates of beta-site amyloid precursor protein-cleaving enzyme (BACE1) and gamma-secretase. *J. Biol. Chem.* **280**, 23009–23017 (2005).
78. K. S. De Jongh, A. A. Colvin, K. K. Wang, W. A. Catterall, Differential proteolysis of the full-length form of the L-type calcium channel alpha 1 subunit by calpain. *J. Neurochem.* **63**, 1558–1564 (1994).
79. N. Gomez-Ospina *et al.*, A promoter in the coding region of the calcium channel gene CACNA1C generates the transcription factor CCAT. *PloS one* **8**, e60526 (2013).
80. J. W. Smyth, R. M. Shaw, Autoregulation of connexin43 gap junction formation by internally translated isoforms. *Cell Rep.* **5**, 611–618 (2013).
81. G. Krapivinsky, L. Krapivinsky, Y. Manasian, D. E. Clapham, The TRPM7 chanzyme is cleaved to release a chromatin-modifying kinase. *Cell* **157**, 1061–1072 (2014).
82. A. A. Bouza *et al.*, Sodium channel β1 subunits participate in regulated intramembrane proteolysis-excitation coupling. *JCI Insight.* **6**, e141776 (2021).
83. D. K. Jones, F. Liu, N. Dombrowski, S. Joshi, G. A. Robertson, Dominant negative consequences of a hERG 1b-specific mutation associated with intrauterine fetal death. *Prog. Biophys. Mol. Biol.* **120**, 67–76 (2016).